Journal of Biomolecular NMR (2006) 36:295–300
DOI 10.1007/s10858-006-9062-5

NMR structure note

Solution structure of calponin homology domain of *Human* MICAL-1

Hongbin Sun, Haiming Dai, Jiahai Zhang, Xianju Jin, Shangmin Xiong, Jian Xu, Jihui Wu* & Yunyu Shi*

From the Hefei National Laboratory for Physical Sciences at Microscale and School of Life Science, University of Science and Technology of China, Hefei, Anhui 230026, People's Republic of China

Received 15 June 2006; Accepted 10 July 2006

Key words: calponin homology domain, MICAL, NMR, residual dipolar couplings, signal transduction

Abbreviations: CH domain – calponin homology domain; MICAL – molecular interacting with CasL protein; MICAL-1 CH – CH domain of *human* MICAL-1; ABD – actin binding domain; ABS – actin binding site; NOE – nuclear Overhauser effect; NOESY – nuclear Overhauser enhancement spectroscopy; COSY – correlated spectroscopy; TOCSY – total correlation spectroscopy; HSQC – heteronuclear single quantum coherence; RMSD – root mean square deviation; LC – liquid crystal.

Biological context

MICALs are a family of proteins conserved in organisms ranging from flies to mammals. MICAL was first identified as CasL (Crk-associated substrate like protein, also known as HEF1) interacting protein and so it was named (Suzuki et al. 2002). Recently, MICALs were found to be a family of proteins expressed in neuron cells, including *Drosophila*-MICAL, *Human*-MICAL-1, *Human*-MICAL-2 and *Human*-MICAL-3. Through interaction with neuronal plexin A (PlexA), MICALs were involved in Semaphorin 1a (Sema-1a) induced repulsive axon guidance (Terman et al. 2002). MICALs were also identified as GTPase rab1 interacting proteins by yeast two-hybrid approach and confirmed by GST pull down experiments (Fischer et al. 2005).

MICALs are a family of conserved multi-domain proteins containing an N-terminal flavoprotein monoxygenase domain, a calponin homology (CH) domain, a LIM domain, a prolin-rich domain, and a coiled-coil motif. CH domain is a protein module of 100–110 residues, which is often found in signaling and cytoskeletal proteins (Gimona et al. 2002; Korenbaum et al. 2002). It is a structurally conserved domain with diverse functions. CH domains often serve as protein–protein interaction domains implicated in signal transduction and cytoskeletal organization (Gimona et al. 2002). Sequence analysis suggest that a single CH domain in proteins is often a type 3 CH domain. However, it may also be a type 2 CH domain such as in MICALs, smoothelin and RP/EBs (Korenbaum et al. 2002). Some of type 2 CH domains can assist the F-actin binding activity of type 1 CH domain (Gimona et al. 2002), regulate protein functions by interacting with phosphatidylinositol (4, 5)-biphosphat (PIP_2) (Fukami et al. 1992), or interact with other cytoskeleton proteins (Berrueta et al. 1998). Yet, the function of CH domain in MICAL-1 remains unknown.

The structure of the N-terminal domain of *Mus musculus* MICAL-1 has been reported and its flavoenzyme activity has been confirmed (Siebold

*To whom correspondence should be addressed. E-mail: wujihui@ustc.edu.cn; yyshi@ustc.edu.cn

et al. 2005; Nadella et al. 2005). The flavoenzyme domain of MICALs is necessary for Sema-1a-PlexA repulsive axon guidance and MICALs are thought to act as protein binding scaffolds to recruit downstream effectors of plexin-mediated responses. However, the downstream effectors of MICALs are still ambiguous. As a potential protein–protein interaction module, CH domain may play an important role in the recruiting of the downstream effectors, such as cytoskeleton molecules. Recently, MICAL-L2 (also known as JARB) was found to interact with rab13 and involved in the dynamic turnover of tight junctions (Terai et al. 2006). MICAL-L2 has a CH domain, LIM domain and C-terminal coiled-coil motif similar to MICALs, but has no the N-terminal flavoenzyme domain. The N-terminal domain of MICAL-L2 (including CH domain and LIM domain) can interact with actin cytoskeleton. However, there was no report available describing the F-actin binding of MICALs. Here, we described the solution structure of CH domain of *human* MICAL-1. Besides, based on the structure and sequence alignment, potential functions of CH domain of *human* MICAL-1 were discussed.

Methods and results

Cloning, expression and purification of the CH domain of human MICAL-1

The DNA fragment encoding residues 506–614 corresponding to the CH domain of *Human* MICAL-1 was amplified from human brain cDNA library (Clontech) by polymerase chain reaction (PCR) using the two primers 5′-CATAT GGGGTCGGCAGGCACCCAG-3′ and 5′-GC-GGCCGCTCACATGCTCTTGAAGGCACTGT GG-3′ designed based on the mRNA sequence of *human* MICAL-1 (Genebank accession No. AB048948). The reaction product (about 350 bp) was purified and then cloned between the *NdeI*/*NotI*-site of p28 (Novagen). The positive clone was identified by DNA sequencing. The recombinant plasmid was then transformed into *Escherichia coli* BL21 (DE3) host cells for expression. Uniformly labeled recombinant human MICAL-1 CH was produced using SV40 medium containing 0.5 g/l 99% ^{15}N ammonium chloride and 2.5 g/l 99% ^{13}C-glucose as the sole nitrogen and carbon source, respectively. Recombinant *human* MICAL-1 CH contains an N-terminal His tag (MGHHHHHHM) and was purified using Ni-chelating column (Qiagen). The purity of recombinant MICAL-1 CH was confirmed by Tricine-SDS-PAGE (15%, w/v) and the concentration was measured with BCA kits (Pierce). The concentrations of ^{15}N-labeled and ^{13}C, ^{15}N-labeled MICAL-1 CH were about 1.5 mM. All the samples for NMR contained 50 mM phosphate buffer (pH 6.5), 50 mM NaCl, and 0.01% sodium azide in 90% H_2O/10% D_2O or in 99.96% D_2O.

NMR spectroscopy and data processing

The NMR experiments were performed on a Bruker DMX500 spectrometer and a Bruker DMX600 spectrometer equipped with cyroprobe. The following spectra were recorded at 293 K to obtain backbone and side chain resonance assignments: 2D ^{1}H, ^{15}N-HSQC, 3D HNCO, HN(CA)CO, CBCA(CO)NH, CBCANH, C(CO)NH-TOCSY, H(CCO)NH-TOCSY, HBHA(CBCACO)NH. The ^{13}C/^{15}N-labeled sample was then lyophilized and dissolved in 99.96% D_2O, which was followed immediately with HSQC experiments to monitor the disappearance of NH signals at 293 K. After most of the peaks vanished, 3D HCCH-TOCSY, HCCH-COSY and ^{13}C-separted NOESY were recorded on this sample at 293 K. Interproton distance restraints were obtained from a 3D ^{15}N-separted NOESY and a ^{13}C-separted NOESY.

$^{1}D_{NH}$ residual dipolar couplings were acquired from the difference in J splittings measured in spectra of aligned (J + D) and isotropic (J) samples using ^{1}H-coupled IPAP {^{15}N, ^{1}H}-HSQC experiments (Ottiger et al. 1998). The LC phage sample contained 17 mg mL^{-1} Pf1 filamentous phage was used as alignment media (Hansen et al. 1998). Approximate values for the axial (Da) and rhombic (R) components of alignment tensor were determined from a histogram of the normalized distribution of $^{1}D_{NH}$ residual dipolar couplings (Clore et al. 1998a). Initial values were Da = 12.5 Hz and R = 0.13. Final values of Da and R were 11.3 and 0.22 refined by performing a grid search program (Clore et al. 1998b).

NMR data processing was carried out using NMRPipe and NMRDraw software, and the data were analyzed with SPARKY. All software was

run on a Linux system. Linear prediction was used to improve spectral resolution in the indirect dimensions where constant-time acquisition was used.

Experimental restraints and NMR structure calculation

NMR distance restraints were collected from cross-peaks in two different NOESY spectra: 3D ^{15}N-separated NOESY in H_2O and 3D ^{13}C-separated NOESY in D_2O. NOE restraints were grouped into four distance ranges: 1.8–3.0 Å for strong peaks; 1.8–4.0 Å for medium peaks; 1.8–5.0 Å for weak peaks; and 1.8–6.0 Å for very weak peaks. Considering that the spin diffusion effect could be serious for aliphatic, a more conservative distance estimation was used for the 3D ^{13}C-separated NOESY; therefore, most medium-range and long-range NOEs from this spectra were put into the weak or very weak groups. The 1.8 Å lower limits were imposed only implicitly by the van der Waals repulsion force. For methyl protons, nonstereospecifically assigned methylene protons, and aromatic ring protons, r^{-6} summation averages were applied. Dihedral angle restraints were calculated from chemical shifts using the program TALOS. Hydrogen bond restraints were obtained by identifying the slow exchange amide protons mainly in the regular secondary structures.

Structures were calculated using the program CNS v1.1, employing a simulated annealing protocol for torsion angle dynamics. For the initial rounds of structure calculations, only sequential, intraresidual, medium-range NOEs, unambiguous long-range NOEs and dihedral angle restraints were used. Later, all other long-range NOEs and hydrogen bonds were introduced in consecutive steps. At last, $^1D_{NH}$ residual dipolar couplings restraints were incorporated into structure determination using the method of Tjandra (Tjandra et al. 1997). Simple impulsion nonbonded interactions were used during structure calculation.

Two hundred structures were calculated, from which the 20 structures with the lowest energies were selected and submitted to PDB. PROCHECK-NMR and MOLMOL were used to validate and to visualize the final structures, respectively.

Structure determination

The recombinant MICAL-1 CH protein was shown to be monomer in solution by gel filtration chromatography experiment. The 2D ^{1}H, ^{15}N-HSQC spectrum of *human* MICAL-1 CH illustrates good dispersion of the proton and nitrogen resonances in amide groups (Figure S1 in supplemental material). In this spectrum, all correlation peaks for the backbone amide resonances were assigned. In total, more than 95% of the side chain resonances were assigned except some side chain resonances of the aromatic rings. Based on the backbone and side chain assignments, the spectra of ^{15}N-edited NOESY and ^{13}C-edited NOESY were assigned and the solution structure of MICAL-1 CH was calculated using CNS. Statistics about the quality and precision of the 20 lowest energies conformers that represent the solution structure of MICAL-1 CH are summarized in Table 1. For the well-structured region from residue Gly4 to Ser108, the RMSD values to the mean structure were 0.46 Å for backbone atoms and 0.89 Å for heavy atoms, which reflect the precision of the structure. The quality of the structure is also reflected by the results from program PROCHECK, in which 88.4% of the residues were in the most favored region on Ramachandran plot, 10.6% in the additionally allowed region, 1.0% in generous allowed region, and no residues in disallowed region. The heavy atoms superimposition of the final 20 conformers in stereo view and a represent structure are shown in Figure 1. In the region between αC and αE helix, there was an increasing level of disorder due to fewer long-range NOEs there.

Structure description

The tertiary structure of MICAL-1 CH consists of six α-helices and one 3_{10} helix and is about totally 67% helical, which is consistent with results obtained from circular dichroism experiment (data not shown). The structure of MICAL-1 CH is dominated by four long α-helices, in which three α-helices, αB (residues 36–45), αD (residues 60–74) and αF (residues 92–108), are assembled into a parallel bundle and the N-terminal helix αA (residues 2–16) packs perpendicularly (Figure 1). The crossing angels between αB and αD, αB and αF are ~20°, while the crossing angel of αA and αB is ~70°. Most of the slowly exchanging NH protons in ^{1}H–^{2}D

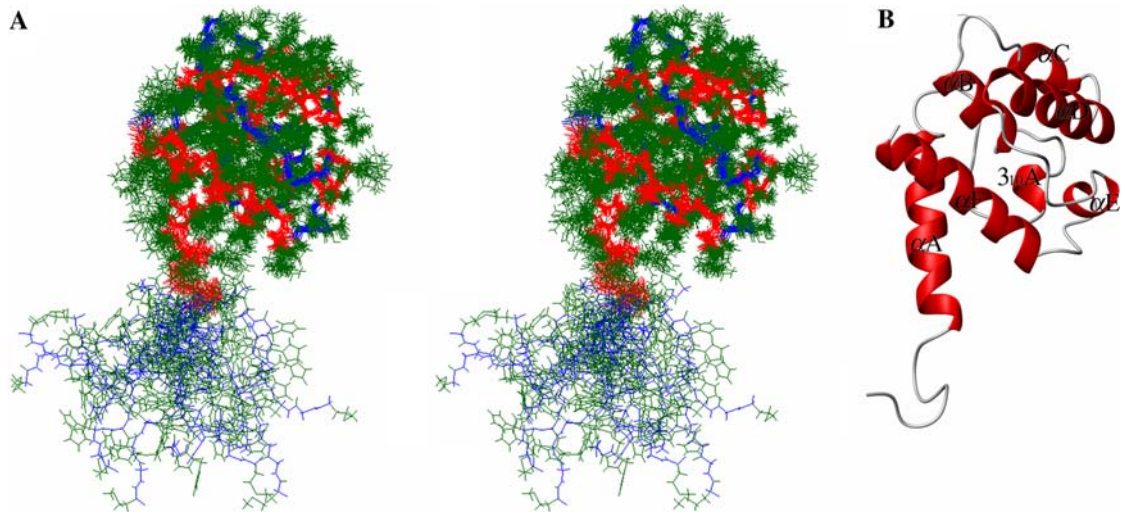

Figure 1. (A) The heavy atoms superposition of 20 lowest-energy conformers from the final CNS calculation of NMR structure of MICAL-1 CH in stereo view. The backbones of helical regions are colored in red, the backbones of remaining residuals are colored in blue and the side-chains are colored in green. (B) A ribbon representation of the minimized average structure with the secondary structure elements highlighted. This figure was produced with MOLMOL.

exchange experiments were also found within these regions, indicating the existence of hydrogen bonds. The four α-helices are connected by two small α-helices, one 3_{10} helix and long loops. The small α-helices are αC (residues 52–58), αE (residues 83–88) and the 3_{10} helix is 3_{10}A (residues 30–32).

By sequence alignment (Figure S2A), many hydrophobic residues were found to be conserved, suggesting that the fold of CH domain is mainly maintained by hydrophobic interactions in the core of the domain. These hydrophobic residues mainly reside in two hydrophobic cores. The first is formed by the packing of helix αA in an almost perpendicular orientation against the central helices αB and αF (Figure 1), including residues are Leu9, Trp12, Ala37, Leu41, Ile96 and Leu99 in MICAL-1 CH, which make a number of van der Waals interactions in this core region. In addition, residue Trp32 in the small 3_{10}A helix also contributes to the core formation. The loop between helix αA and 3_{10}A is linked to the protein body by van der Waals interaction between residue Val25 and the first hydrophobic core. Another hydrophobic core is buried in the bundle formed by helices αB, αD and αF. The residues involved are Leu38, Val42, Leu68, Ala71, Tyr98 and Phe102, which also make a number of van der Waals interactions. Helix E makes a hydrophobic interaction with this hydrophobic core through residue Val86. Their hydrophobic character tends to be conserved in all CH domains. Residue P47 in MICAL-1 CH is also conserved (Gly in type 1 CH domain), which can be explained by the formation of a helical turn (Figure S2A).

Discussion and conclusion

Structure comparison with other structures of CH domains

Structures have been solved for the CH domains in many proteins, including actinin (Franzot et al. 2005), dystrophin (Keep et al. 1999) and so on. Structural comparison between MICAL-1 CH and other representative CH domains extends our understanding of subtle differences in structure. Although the amino acid sequence identities between MICAL-1 CH domain and other CH domains are lower than 35%, their structures are very similar. The structure of MICAL-1 CH (2DK9) also indicates a type 2 CH domain, justified by the fact that RMSDs with CH2 domain of 1QAG and 1WKU are 1.6 and 1.8 Å, respectively, while RMSDs with type 1 CH domains of 1QAG and 1WKU are 2.3 and 2.1 Å, respectively. The most prominent structural difference is the crossing angel between the first helix and the third helix

Table 1. Structural statistics for the selected 20 structures of MICAL1 CH domain[a]

Number of NMR restraints used in the structure calculation	
Intra-residue	534
Sequential ($\|i-j\| = 1$)	515
Medium-range ($1 < \|i-j\| < 5$)	406
Long-range ($\|i-j\| \geq 5$)	291
Total NOE restraints	1746
Hydrogen bonds	82
Dihedral angle restraints	140
Residual dipolar couplings restraints	74
Lennard-Jones potential energy (kcal mol^{-1})	-220.86 ± 16.80
RMSD from idealized covalent geometry	
Bonds (Å)	0.0008 ± 0.00003
Angles (deg)	0.2876 ± 0.0015
Impropers (deg)	0.1208 ± 0.0043
RMSD from experimental restraints	
Distance (Å)	0.0027 ± 0.0003
cdih (deg)	0.1539 ± 0.0173
Coordinate RMSD from mean (Å) residues 4–108	
All backbone atoms	0.463
All heavy atoms	0.885
Ramachandran plot (% residues 1–109)	
Residues in most favored regions	88.4
Residues in additional allowed regions	10.6
Residues in generously allowed regions	1.0
Residues in disallowed regions	0.0

[a]None of the structure exhibits distance violations greater than 0.2 Å or dihedral angle violations greater than 2°.

of these structures. In MICAL-1 CH, the angel is about 70°, while in 1QAG CH1, 1WKU CH1, 1QAG CH2, 1WKU CH2, they are 53°, 57°, 77°, and 74°, respectively. The cross angels of the first helix and the third helix in type 2 CH domains are obviously larger than those in type 1 CH domains. Another obviously difference is in type 2 CH domains, the fifth helix (15 residues) is shorter than that in type 1 CH domains (17 residues).

Possible functions of MICAL-1 CH domain

The functions of MICALs are far from clear. One most important progress indicates that the flavoenzyme domain of MICALs is necessary for Sema-1a-PlexA repulsive axon guidance and MICALs may act as protein binding scaffolds to recruit downstream effectors of plexin-mediated responses (Terman et al. 2002). As a potential protein–protein interaction module, CH domain may play an important role in the recruiting activities, possibly recruiting cytoskeleton molecules. In many proteins, a type 2 CH domain combines with a type 1 CH domain to form an actin binding module in which the type 1 CH domain alone can bind F-actin while the type 2 CH domain alone can not and only assists the binding (Winder et al. 1995; Djinovic-Carugo et al. 1997). In smoothelin, RP/EBs and MICALs, there is only one CH domain, which belongs to type 2. In order to know whether F-actin can bind to MICAL-1 CH domain, we used 2D ^{1}H, ^{15}N-HSQC to monitor the interaction between MICAL-1 CH and F-actin by titration. No obvious change was observed. It seems MICAL-1 CH domain cannot bind to F-actin. Although the structure of MICAL-1 CH (2DK9) is similar to other CH domains, including type 1 CH domains, there are many differences in their hydrophobic surfaces (Figure S2B–D). The long αG helix in the C terminal of CH1 domain in α-actinin (Franzot et al. 2005), which is thought to be actin binding site 2 (ABS2), is not conserved in MICAL-1 CH domain (αF in MICAL-1 CH). There are many hydrophobic residues in the long αG helix of the CH1 domains of α-actinin which is thought to interact with F-actin through hydrophobic forces (Gimona et al. 2002). However, in the CH domain of MICAL-1, these residues are replaced by many hydrophilic residues, such as S100, H101, H103, S104, K107 and S108. The residue Lys49 in the N-terminal helix of the CH1 domain of α-actinin, which is important for F-actin binding, is replaced by Glu in MICAL-1 CH domain (Figure S2A). These observations might explain why a type 2 CH domain in MICAL-1 alone is not able to bind to F-actin.

Suzuki et al. observed that vimentin bound to CH domain of MICAL-1 in GST pull down experiments, but CH domain was not necessary for the interaction between MICAL-1 and vimentin *in vivo* (Suzuki et al. 2002). However, Fischer et al. performed immunofluorescence analysis and yeast two-hybridization and they did not detect the binding of MICAL-1 to vimentin

(Fischer et al. 2005). We also performed GST pull down experiments, and the binding between CH domain of MICAL-1 and vimentin could not be observed. Since controversial data exists, the question remains to be answered. Many hydrophobic residues are observed in the surface of MICAL-1 CH, which may easily have hydrophobic interactions with other proteins and domains. MICAL-1 CH may serve as a module to mediate interaction with other proteins or to enhance the interaction affinity. Recently, the cellular localization of MICAL proteins was reported to be relevant to the microtubule cytoskeleton (Fischer et al. 2005). Considering that RP/EB family proteins interact with microtubule cytoskeleton through their type 2 CH domains (Juwana et al. 1999), it is possible that MICALs interact with microtubule cytoskeleton through their CH domains.

Conclusion

Here we report the three-dimensional structure of the calponin homology domain of human MICAL-1 determined by nuclear magnetic resonance methods based on NOEs and residual dipolar couplings experiments. Although the amino acid sequence identities between MICAL-1 CH domain and other CH domains are lower than 35%, the structure shares the common feature of other CH domains. Structure alignment and hydrophobic surface analysis prove that MICAL-1 CH domain is a type 2 CH domain.

Protein Data Bank accession number

The coordinates of the 20 structures of CH domain of human MICAL-1 (506–614) with the lowest energies were selected and deposited in the Protein Data Bank (PDB entry 2DK9). The NMR chemical shifts were deposited in BioMagResBank (BMRB), accession number: 7058.

Acknowledgments

This work was supported by the Chinese National Fundamental Research Project (Grant 2002CB713806 and 2004CB520800), the Chinese National Natural Science Foundation (Grant 30270293, 30121001 and 30570361), the Key Project of the National High Technology Research and Development Program of China (Grant 2002BA711A13), and the Pilot Project of the Knowledge Innovation Program of the Chinese Academy of Science (Grant KSCX1-SW-17).

Electronic Supplementary Material is available to authorized users in the online version of this article at http://www.dx.doi.org/10.1007/s10858-006-9062-5

References

Berrueta, L., Kraeft, S.K., Tirnauer, J.S., Schuyler, S.C., Chen, L.B., Hill, D.E., Pellman, D. and Bierer, B.E. (1998) *Proc. Natl. Acad. Sci.*, **95**, 10596–10601.

Clore, G.M., Gronenborn, A.M. and Bax, A. (1998a) *J. Magn. Reson.*, **133**, 216–221.

Clore, G.M., Gronenborn, A.M. and Tjandra, N. (1998b) *J. Magn. Reson.*, **131**, 159–162.

Djinovic-Carugo, K., Banuelos, S. and Saraste, M. (1997) *Nat. Struct. Biol.*, **4**, 175–179.

Fischer, J., Weide, T. and Barnekow, A. (2005) *Biochem. Biophys. Res. Commun.*, **328**, 415–423.

Franzot, G., Sjoblom, B., Gautel, M. and Djinovic-Carugo, K. (2005) *J. Mol. Biol.*, **348**, 151–165.

Fukami, K., Furuhashi, K., Inagaki, M., Endo, T., Hatano, S. and Takenawa, T. (1992) *Nature*, **359**, 150–152.

Gimona, M., Djinovic-Carugo, K., Kranewitter, W.J. and Winder, S.J (2002) *FEBS Lett.*, **513**, 98–106.

Hansen, M.R., Mueller, L. and Pardi, A. (1998) *Nat. Struct. Biol.*, **5**, 1065–1074.

Juwana, J.P., Henderikx, P., Mischo, A., Wadle, A., Fadle, N., Gerlach, K., Arends, J.W., Hoogenboom, H., Pfreundschuh, M. and Renner, C. (1999) *Int. J. Cancer*, **81**, 275–284.

Keep, N.H., Winder, S.J., Moores, C.A., Walke, S., Norwood, F.L. and Kendrick-Jones, J. (1999) *Structure*, **7**, 1539–1546.

Korenbaum, E. and Rivero, F. (2002) *J. Cell Sci.*, **115**, 3543–3545.

Nadella, M., Bianchet, M.A., Gabelli, S.B., Barrila, J. and Amzel, L.M. (2005) *Proc. Natl. Acad. Sci.*, **102**, 16830–16835.

Ottiger, M., Delaglio, F. and Bax, A. (1998) *J. Magn. Reson.*, **131**, 373–378.

Siebold, C., Berrow, N., Walter, T.S., Harlos, K., Owens, R.J., Stuart, D.I., Terman, J.R., Kolodkin, A.L., Pasterkamp, R.J. and Jones, E.Y. (2005) *Proc. Natl. Acad. Sci.*, **102**, 16836–16841.

Suzuki, T., Nakamoto, T., Ogawa, S., Seo, S., Matsumura, T., Tachibana, K., Morimoto, C. and Hirai, H (2002) *J. Biol. Chem.*, **277**, 14933–14941.

Terai, T., Nishimura, N., Kanda, I., Yasui, N. and Sasaki, T (2006) *Mol. Biol. Cell*, **17**, 2465–2475.

Terman, J.R., Mao, T., Pasterkamp, R.J., Yu, H.H. and Kolodkin, A.L (2002) *Cell*, **109**, 887–900.

Tjandra, N., Omichinski, J.G., Gronenborn, A.M., Clore, G.M. and Bax, A (1997) *Nat. Struct. Biol.*, **4**, 732–738.

Winder, S.J., Hemmings, L., Maciver, S.K., Bolton, S.J., Tinsley, J.M., Davies, K.E., Critchley, D.R. and Kendrick-Jones, J. (1995) *J. Cell Sci.*, **108**, 63–71.